2009

Beyond Molecular Recognition: Using a Repulsive Field to Tune Interfacial Valency and Binding Specificity between Adhesive Surfaces

Maria M. Santore
University of Massachusetts Amherst

Jun Zhang
University of Massachusetts Amherst

Sudhanshu Srivastava
University of Massachusetts Amherst

Vincent M. Rotello
University of Massachusetts Amherst

Recommended Citation

Santore, Maria M.; Zhang, Jun; Srivastava, Sudhanshu; and Rotello, Vincent M., "Beyond Molecular Recognition: Using a Repulsive Field to Tune Interfacial Valency and Binding Specificity between Adhesive Surfaces" (2009). *Langmuir*. 152.
https://doi.org/10.1021/la802554s

Invited Feature Article

Beyond Molecular Recognition: Using a Repulsive Field to Tune Interfacial Valency and Binding Specificity between Adhesive Surfaces

Maria M. Santore,*,† Jun Zhang,† Sudhanshu Srivastava,‡ and Vincent M. Rotello‡

Department of Polymer Science and Engineering and Department of Chemistry, University of Massachusetts, Amherst, Massachusetts 01003

Received August 6, 2008. Revised Manuscript Received September 11, 2008

Surface-bound biomolecular fragments enable "smart" materials to recognize cells and other particles in applications ranging from tissue engineering and medical diagnostics to colloidal and nanoparticle assembly. Such smart surfaces are, however, limited in their design to biomolecular selectivity. This feature article demonstrates, using a completely nonbiological model system, how specificity can be achieved for particle (and cell) binding, employing surface designs where immobilized nanoscale adhesion elements are entirely nonselective. Fundamental principles are illustrated by a model experimental system where 11 nm cationic nanoparticles on a planar negative silica surface interact with flowing negative silica microspheres having 1.0 and 0.5 μm diameters. In these systems, the interfacial valency, defined as the number of cross-bonds needed to capture flowing particles, is tunable through ionic strength, which alters the range of the background repulsion and therefore the effective binding strength of the adhesive elements themselves. At high ionic strengths where long-range electrostatic repulsions are screened, single surface-bound nanoparticles capture microspheres, defining the univalent regime. At low ionic strengths, competing repulsions weaken the effective nanoparticle adhesion so that multiple nanoparticles are needed for microparticle capture. This article discusses important features of the univalent regime and then illustrates how multivalency produces interfacial-scale selectivity. The arguments are then generalized, providing a possible explanation for highly specific cell binding in nature, despite the degeneracy of adhesion molecules and cell types. The mechanism for the valency-related selectivity is further developed in the context of selective flocculation in the colloidal literature. Finally, results for multivalent binding are contrasted with the current thinking for interfacial design and the presentation of adhesion moieties on engineered surfaces.

Introduction

In the bionanotechnology revolution, biomolecular fragments immobilized on synthetic surfaces enable highly specific binding to target particles and cells. Applications include drug delivery by stealth liposomes[1−5] and "smart" carriers,[6−11] tissue engineering on functionalized scaffolds,[12−21] sensors,[22−25] cell sorting,[26,27] and diagnostics.[28−30] Immobilized and tethered biomolecules also direct the assembly of colloidal- and nanoparticle-based hierarchical materials.[31−41] Popular molecules that facilitate binding specificity include DNA strands and antibodies

* Corresponding author. E-mail: santore@mail.pse.umass.edu.
† Department of Polymer Science and Engineering.
‡ Department of Chemistry.

(1) Gabizon, A.; Horowitz, A. T.; Goren, D.; Tzemach, D.; Mandelbaum-Shavit, F.; Qazen, M. M.; Zalipsky, S. *Bioconjugate Chem.* **1999**, *10*, 289–298.
(2) Lasic, D. D. *Trends Biotechnol.* **1998**, *16*, 307–321.
(3) Torchilin, V. P. *J. Microencapsul.* **1998**, *15*, 1–19.
(4) Harding, J. A.; Engbers, C. M.; Newman, M. S.; Goldstein, N. I.; Zalipsky, S. *Biochim. Biophys. Acta* **1997**, *1327*, 181–192.
(5) Zalipsky, S. *Adv. Drug Delivery Rev.* **1995**, *16*, 157–182.
(6) Pantel, K.; Cote, R. J.; Fodstad, O. *J. Natl. Cancer Inst.* **1999**, *91*, 1113–1124.
(7) Bes, L.; Angot, S.; Limer, A.; Haddleton, D. M. *Macromolecules* **2003**, *36*, 2493–2499.
(8) Moghimi, S. M.; Hunter, A. C.; Murray, J. C. *Pharmacol. Rev.* **2001**, *53*, 283–318.
(9) Vyas, S. P.; Singh, A.; Sihorkar, V. *Crit. Rev. Ther. Drug Carrier Syst.* **2001**, *18*, 1–76.
(10) Hashida, M.; Hirabayashi, H.; Nishikawa, M.; Takakura, Y. *J. Controlled Release* **1997**, *46*, 129–137.
(11) Saiki, I.; Yoneda, J.; Igarashi, Y.; Aoki, M.; Kusunose, N.; Ono, K. I.; Azuma, I. *Jpn. J. Cancer Res.* **1993**, *84*, 558–565.
(12) Casper, C. L.; Yamaguchi, N.; Kiick, K. L.; Rabolt, J. F. *Biomacromolecules* **2005**, *6*, 1998–2007.
(13) Fan, V. H.; Au, A.; Tamama, K.; Littrell, R.; Richardson, L. B.; Wright, J. W.; Wells, A.; Griffith, L. G. *Stem Cells* **2007**, *25*, 1241–1251.
(14) Ishihara, M.; Sato, M.; Hattori, H.; Saito, Y.; Yura, H.; Ono, K.; Masuoka, K.; Kikuchi, M.; Fujikawa, K.; Kurita, A. *J. Biomed. Mater. Res.* **2001**, *56*, 536–544.
(15) Mann, B. K.; Tsai, A. T.; Scott-Burden, T.; West, J. L. *Biomaterials* **1999**, *20*, 2281–2286.
(16) Mann, B. K.; Schmedlen, R. H.; West, J. L. *Biomaterials* **2001**, *22*, 439–444.
(17) Seal, B. L.; Panitch, A. *Biomacromolecules* **2003**, *4*, 1572–1582.
(18) Schussler, O.; Coirault, C.; Louis-Tisserand, M.; Ei-Chare, W.; Oliviero, P.; Menard, C.; Michelot, R.; Salomon, D. R.; Chachques, J. C.; Carpentier, A.; Lecarpentier, Y. *Circulation* **2007**, *116*, 70–70.
(19) Massia, S. P.; Hubbell, J. A. *Anal. Biochem.* **1990**, *187*, 292–301.
(20) Glass, J. R.; Dickerson, K. T.; Stecker, K.; Polarek, J. W. *Biomaterials* **1996**, *17*, 1101–1108.
(21) Chung, A. S.; Gao, Q.; Kao, W. J. *J. Biomater. Sci., Polym. Ed.* **2007**, *18*, 713–729.
(22) Ilic, B.; Czaplewski, D.; Zalalutdinov, M.; Craighead, H. G.; Neuzil, P.; Campagnolo, C.; Batt, C. *J. Vac. Sci. Technol., B* **2001**, *19*, 2825–2828.
(23) Shipway, A. N.; Katz, E.; Willner, I. *ChemPhysChem* **2000**, *1*, 18–52.
(24) Ilic, B.; Czaplewski, D.; Craighead, H. G.; Neuzil, P.; Campagnolo, C.; Batt, C. *Appl. Phys. Lett.* **2000**, *77*, 450–452.
(25) Ivnitski, D.; Abdel-Hamid, I.; Atanasov, P.; Wilkins, E. *Biosens. Bioelectron.* **1999**, *14*, 599–624.
(26) Narasipura, S. D.; Wojciechowski, J. C.; Charles, N.; Liesveld, J. L.; King, M. R. *Clin. Chem.* **2008**, *54*, 77–85.
(27) Nagrath, S.; Sequist, L. V.; Maheswaran, S.; Bell, D. W.; Irimia, D.; Ulkus, L.; Smith, M. R.; Kwak, E. L.; Digumarthy, S.; Muzikansky, A.; Ryan, P.; Balis, U. J.; Tompkins, R. G.; Haber, D. A.; Toner, M. *Nature* **2007**, *450*, 1235–U1210.
(28) Zhu, H.; Macal, M.; Jones, C. N.; George, M. D.; Dandekar, S.; Revzin, A. *Anal. Chim. Acta* **2008**, *608*, 186–196.
(29) Bailey, R. C.; Kwong, G. A.; Radu, C. G.; Witte, O. N.; Heath, J. R. *J. Am. Chem. Soc.* **2007**, *129*, 1959–1967.
(30) Miettinen, M.; Virolainen, M.; Maaritsarlomorikala, *Am. J. Surg. Pathol.* **1995**, *19*, 207–216.

10.1021/la802554s CCC: $40.75
Published on Web 10/31/2008

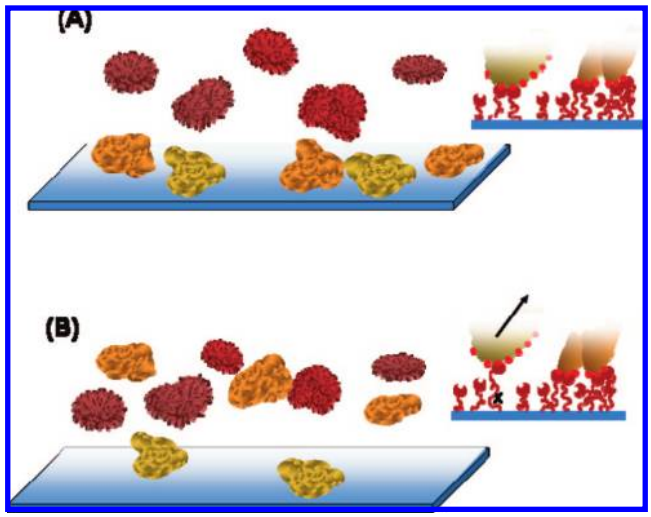

Figure 1. (A). Current state of the art where recognition by immobilized biomolecular fragments adheres all ligand-presenting cells. (B) Future biomaterial where additional surface design features discriminate between secondary features on ligand-presenting cells while still rejecting cells not containing target ligands.

or antibody fragments. In these technologies, molecular-level specificity translates directly to the microscale or cellular level as long as (1) the biomolecules on the engineered surface are accessible to those on the target object and (2) surfaces are passivated to eliminate nonspecific interactions that could adhere nontarget objects. Whereas the translation from molecular recognition to a 1:1 pairing of targeted surfaces works well, the approach is limited in that it reflects the perspective that the role of the surface is simply to present biomolecules in a fashion that preserves their solution binding properties. More sophisticated dynamic functionality could be realized by incorporating elegant surface design principles (Figure 1). For instance, one might wish to discriminate targets (cells) based not only on the presence of a particular surface marker but also on its surface arrangement or concentration. One might also wish to employ synthetic rather than biological molecules (for reasons of cost effectiveness or chemical robustness) that possess some molecular-scale selectivity but lack the extreme molecular specificity of DNA or antibodies. Both the sensitivity to surface features and relaxation of the perfect molecular specificity criterion are found in natural systems, making them excellent prototypes for designing synthetic nanosystems.

Inspiration from Biology. From our perspective, cell surfaces hold the key to material design principles for interfaces with highly specific and sophisticated dynamic function. The fabrication of advanced biomimetically functional surfaces need not involve a greater expense than already associated with the production of surfaces functioning by simple molecular recognition; however, the underlying principles need to be better understood. In particular, we are interested in how the properties of the entire surface can be engineered to exceed the performance of the individual molecules.

When Nature brings together microscale surfaces, the pairing between a biomolecular substrate and its target does not translate to exclusive pairing between particular cell types. Additionally, the adhesion molecules responsible for cellular interactions can be less specific in their targeting than the antibodies and DNA employed in "bionanotechnologies." (Indeed, these particular molecules tend not to be used in nature: antibodies work within the immune system whereas DNA binding occurs at the molecular rather than interfacial level in the nucleus.) Each cell presents many different adhesion molecules, and whereas their molecular detail is somewhat tissue-specific,[42−44] a few basic types of adhesion molecules appear on many different types of cells.[44−50] Furthermore, the degeneracy in the binding partners for each adhesion molecule is becoming increasingly appreciated.[42,43] For example, P-selectin, found on platelets, is also expressed on the vascular endothelium in response to an injury.[51−53] Like E-selectin and L-selectin, P-selectin binds sialyl Lewis^x groups[54] but also binds PSGL-1 and CD24 on leukocytes[54] and sialylated, fucosylated lactosaminoglycans on myeloid cells.[55] Likewise, ICAM-1, found on vascular endothelium, binds beta-2 integrins on neutrophils in the inflammatory response[43] but also binds CD43, rhinoviruses, and fibrinogen.[47,48] Finally, the RGD (Arg-Gly-Asp) peptide sequence is a universal motif responsible for cell attachment to the extracellular matrix in addition to blood cell interactions: over half of the known integrins recognize this sequence.[56,57] Despite the fact that the similar adhesion molecules appear on a variety of cells, cells manage to adhere to their targets in a highly specific and dynamically appropriate fashion.

Valency in the Laboratory. Of the mechanisms that enable cells to accomplish precise targeting between opposing surfaces, this article explores the principle of interfacial multivalency, a concept that can be readily translated to the design of synthetic surfaces. Just as it is now recognized that molecular-level binding in solution, or the binding between single solvated molecules and a surface, differs substantially from the binding physics between two surfaces bearing immobilized adhesion molecules,[58−64] we make a distinction here between molecular-level multivalency (terminology of the pharmaceutical chemist) and

(31) Shyr, M. H. S.; Wernette, D. P.; Wiltzius, P.; Lu, Y.; Braun, P. V. *J. Am. Chem. Soc.* **2008**, *130*, 8234–8240.
(32) Strable, E.; Johnson, J. E.; Finn, M. G. *Nano Lett.* **2004**, *4*, 1385–1389.
(33) Chakrabarti, R.; Klibanov, A. M. *J. Am. Chem. Soc.* **2003**, *125*, 12531–12540.
(34) Niemeyer, C. M.; Ceyhan, B.; Noyong, M.; Simon, U. *Biochem. Biophys. Res. Commun.* **2003**, *311*, 995–999.
(35) Boal, A. K.; Rotello, V. M. *J. Am. Chem. Soc.* **2000**, *122*, 734–735.
(36) Hiddessen, A. L.; Rodgers, S. D.; Weitz, D. A.; Hammer, D. A. *Langmuir* **2000**, *16*, 9744–9753.
(37) Boal, A. K.; Rotello, V. M. *J. Am. Chem. Soc.* **1999**, *121*, 4914–4915.
(38) Mirkin, C. A.; Letsinger, R. L.; Mucic, R. C.; Storhoff, J. J. *Nature* **1996**, *382*, 607–609.
(39) Bayraktar, H.; Srivastava, S.; You, C. C.; Rotello, V. M.; Knapp, M. J. *Soft Matter* **2008**, *4*, 751–756.
(40) Milam, V. T.; Hiddessen, A. L.; Crocker, J. C.; Graves, D. J.; Hammer, D. A. *Langmuir* **2003**, *19*, 10317–10323.
(41) Parak, W. J.; Gerion, D.; Pellegrino, T.; Zanchet, D.; Micheel, C.; Williams, S. C.; Boudreau, R.; Le Gros, M. A.; Larabell, C. A.; Alivisatos, A. P. *Nanotechnology* **2003**, *14*, R15−R27.
(42) Salmi, M.; rew, D. P.; Butcher, E. C.; Jalkanen, S. *J. Exp. Med.* **1995**, *181*, 137–149.
(43) Albelda, S. M.; Smith, C. W.; Ward, P. A. *FASEB J.* **1994**, *8*, 504–512.
(44) Murray, B. A.; Owens, G. C.; Prediger, E. A.; Crossin, K. L.; Cunningham, B. A.; Edelman, G. M. *J. Cell Biol.* **1986**, *103*, 1431–1439.
(45) Obrien, K. D.; Allen, M. D.; McDonald, T. O.; Chait, A.; Harlan, J. M.; Fishbein, D.; McCarty, J.; Ferguson, M.; Hudkins, K.; Benjamin, C. D.; Lobb, R.; Alpers, C. E. *J. Clinical Invest.* **1993**, *92*, 945–951.
(46) Hirsch, M. R.; Gaugler, L.; Deagostinibazin, H.; Ballycuif, L.; Goridis, C. *Mol. Cell. Biol.* **1990**, *10*, 1959–1968.
(47) Simmons, D.; Makgoba, M. W.; Seed, B. *Nature* **1988**, *331*, 624–627.
(48) vandeStolpe, A.; vanderSaag, P. T. *J. Mol. Med.* **1996**, *74*, 13–33.
(49) Hoffmann, I.; Balling, R. *Dev. Biol.* **1995**, *169*, 337–346.
(50) Rutishauser, U.; Acheson, A.; Hall, A. K.; Mann, D. M.; Sunshine, J. *Science* **1988**, *240*, 53–57.
(51) Tedder, T. F.; Steeber, D. A.; Chen, A.; Engel, P. *FASEB J.* **1995**, *9*, 866–873.
(52) Varki, A. *Proc. Natl. Acad. Sci. U.S.A.* **1994**, *91*, 7390–7397.
(53) McEver, R. P.; Beckstead, J. H.; Moore, K. L.; Marshallcarlson, L.; Bainton, D. F. *J. Clin. Invest.* **1989**, *84*, 92–99.
(54) Foxall, C.; Watson, S. R.; Dowbenko, D.; Fennie, C.; Lasky, L. A.; Kiso, M.; Hasegawa, A.; Asa, D.; Brandley, B. K. *J. Cell. Biol.* **1992**, *117*, 895–902.
(55) Moore, K. L.; Stults, N. L.; Diaz, S.; Smith, D. F.; Cummings, R. D.; Varki, A.; McEver, R. P. *J. Cell. Biol.* **1992**, *118*, 445–456.
(56) Buck, C. A.; Horwitz, A. F. *Annu. Rev. Cell. Biol.* **1987**, *3*, 179–205.
(57) Ruoslahti, E.; Pierschbacher, M. D. *Science* **1987**, *238*, 491–497.
(58) Bell, G. I. *Science* **1978**, *200*, 618–627.

the interfacial multivalency relevant to materials design and surface−surface interactions. Molecular-level multivalency is a property of individual adhesion moieties whereas interfacial multivalency counts the number of cross-bonds between two approaching surfaces. The latter is influenced not only by the identities of the immobilized ligands but also by their presentation and arrangement on a surface along with other surface features.

When designing surfaces whose functions rely on immobilized adhesion molecules, the first obvious consideration is the character of the adhesion molecules themselves. Besides specificity, binding strength is critically important. The majority of cellular adhesion molecules bind with energies near $10kT$, making the individual bonds reversible.[65−67] Also worth mentioning is the importance of the binding kinetics. Binding and unbinding rate constants comprise a "state space" in which different families of adhesion molecules reside and accomplish their function.[68,69] Additionally, the sensitivity of the binding rates to external forces[64,70] is implicated in some unusual behavior, for instance, catch-stick or catch-slip bonds,[71−75] and the shear threshold observed for L-selectin.[76−79] This quantitative focus on the interfacial reaction rate constants of immobilized adhesion molecules is a relatively recent development within the biophysics community, and it has yet to impact materials design.

The concept of valency is closely tied to binding strength: when single reversible weak bonds cannot hold a molecule, particle, or cell in place, many such interactions may suffice. The utility of multiple weak bonds, however, goes beyond the obvious additive increase in binding energy. Even the grouping of two peptide binding sequences into a single dimer can increase the binding constant several orders of magnitude relative to that of the individual peptides.[80] Likewise, antibody-presenting nanoparticles substantially exceed the affinity of the original monoclonal antibodies.[81] Following the general principle that multiple low-affinity contacts produce high-avidity overall binding, the placement of multiple functionality on single molecules,[82−84] polymers,[85−87] nanoparticles,[88−92] micelles,[93] and dendrimers[94,95] has comprised a molecular-level strategy to target pharmaceutical agents.

Valency on the Cell. Biologists employ a different use of the term "multivalent" to describe multiple contacts between biological cells. Like the chemists' definition, the biological perspective is related to the need for multiple bonds when the weak individual bonds are reversible.[96−98] It is less clear, however, that multiple cross-bonds, for instance, between cells, translate to a greater binding constant because one typically does not define a binding constant at the cellular level. Nonetheless, important biological behaviors are enabled by cell-level or, more broadly in our view, "interfacial multivalency".[96,97] As an example, the viral infection of cells is considered to be multivalent because it has typically been found to involve at least 10 cellular receptors.[99] Greater numbers of bonds typically drive adhesion between mammalian cells. Indeed, the immune system exploits a threshold in the number of bonds that will activate a T-lymphocyte,[100−103] allowing cells of the host to be discriminated from foreign threats. The number of bonds that form between cells also influences their dynamic behavior. For instance, the rolling of leukocytes on injury-activated endothelium is sustained by the reversible engagement of 20−100 selectin bonds.[104,105] Fewer bonds produce tethering.[76] It is also recognized that variations in the selectin density on the vascular endothelium of different tissues render cancer metastasis selective.[106−110] For instance, small cell carcinomas of the lung typically spread to the brain whereas prostate cancer cells spread mostly to bone.[110] Even at the microscale on the surface of single vascular endothelial cells, higher concentrations of selectins near cell junctions have been found to play an important role in transmigration and, more recently, have been recognized to influence the early stages of leukocyte binding.[111]

(59) Leckband, D. E.; Schmitt, F. J.; Israelachvili, J. N.; Knoll, W. *Biochemistry* **1994**, *33*, 4611–4624.
(60) Florin, E. L.; Moy, V. T.; Gaub, H. E. *Science* **1994**, *264*, 415–417.
(61) Jeppesen, C.; Wong, J. Y.; Kuhl, T. L.; Israelachvili, J. N.; Mullah, N.; Zalipsky, S.; Marques, C. M. *Science* **2001**, *293*, 465–468.
(62) Evans, E.; Ritchie, K. *Biophys. J.* **1997**, *72*, 1541–1555.
(63) Bell, G. I.; Dembo, M.; Bongrand, P. *Biophys. J.* **1984**, *45*, 1051–1064.
(64) Merkel, R.; Nassoy, P.; Leung, A.; Ritchie, K.; Evans, E. *Nature* **1999**, *397*, 50–53.
(65) Moore, N. W.; Mulder, D. J.; Kuhl, T. L. *Langmuir* **2008**, *24*, 1212–1218.
(66) Wang, R. X.; Fang, X. L.; Lu, Y. P.; Wang, S. M. *J. Med. Chem.* **2004**, *47*, 2977–2980.
(67) Wang, R. X.; Fang, X. L.; Lu, Y. P.; Yang, C. Y.; Wang, S. M. *J. Med. Chem.* **2005**, *48*, 4111–4119.
(68) Korn, C. B.; Schwarz, U. S. *Phys. Rev. E* **2008**, 77.
(69) Bhatia, S. K.; King, M. R.; Hammer, D. A. *Biophys. J.* **2003**, *84*, 2671–2690.
(70) Evans, E.; Ritchie, K. *Biophys. J.* **1999**, *76*, 2439–2447.
(71) Hammer, D. A. *Curr. Biol.* **2005**, *15*, R96−R99.
(72) Caputo, K. E.; Lee, D.; King, M. R.; Hammer, D. A. *Biophys. J.* **2007**, *92*, 787–797.
(73) Liu, F.; Ou-Yang, Z. C. *Phys. Rev. E* **2006**, 74.
(74) Pereverzev, Y. V.; Prezhdo, O. V. *Biophys. J.* **2006**, *91*, L19−L21.
(75) Marshall, B. T.; Long, M.; Piper, J. W.; Yago, T.; McEver, R. P.; Zhu, C. *Nature* **2003**, *423*, 190–193.
(76) Schwarz, U. S.; Alon, R. *Proc. Natl. Acad. Sci. U.S.A.* **2004**, *101*, 6940–6945.
(77) Dwir, O.; Solomon, A.; Mangan, S.; Kansas, G. S.; Schwarz, U. S.; Alon, R. *J. Cell Biol.* **2003**, *163*, 649–659.
(78) Lawrence, M. B.; Kansas, G. S.; Kunkel, E. J.; Ley, K. *J. Cell. Biol.* **1997**, *136*, 717–727.
(79) Finger, E. B.; Puri, K. D.; Alon, R.; Lawrence, M. B.; vonAndrian, U. H.; Springer, T. A. *Nature* **1996**, *379*, 266–269.
(80) Tweedle, M. F. *Contrast Media Mol. Imaging* **2006**, *1*, 2–9.
(81) Soukka, T.; Harma, H.; Paukkunen, J.; Lovgren, T. *Anal. Chem.* **2001**, *73*, 2254–2260.
(82) Mazzaglia, A.; Forde, D.; Garozzo, D.; Malvagna, P.; Ravoo, B. J.; Darcy, R. *Org. Biomol. Chem.* **2004**, *2*, 957–960.
(83) Gestwicki, J. E.; Cairo, C. W.; Strong, L. E.; Oetjen, K. A.; Kiessling, L. L. *J. Am. Chem. Soc.* **2002**, *124*, 14922–14933.
(84) Kiessling, L. L.; Gestwicki, J. E.; Strong, L. E. *Curr. Opin. Chem. Biol.* **2000**, *4*, 696–703.
(85) Fabre, J. W.; Collins, L. *Curr. Gene Ther.* **2006**, *6*, 459–480.
(86) Kiessling, L. L.; Pohl, N. L. *Chem. Biol.* **1996**, *3*, 71–77.
(87) Mortell, K. H.; Weatherman, R. V.; Kiessling, L. L. *J. Am. Chem. Soc.* **1996**, *118*, 2297–2298.
(88) Boal, A. K.; Rotello, V. M. *J. Am. Chem. Soc.* **2002**, *124*, 5019–5024.
(89) Thoma, G.; Streiff, M. B.; Katopodis, A. G.; Duthaler, R. O.; Voelcker, N. H.; Ehrhardt, C.; Masson, C. *Chem.−Eur. J.* **2005**, *12*, 99–117.
(90) Nolting, B.; Yu, J. J.; Liu, G. Y.; Cho, S. J.; Kauzlarich, S.; Gervay-Hague, J. *Langmuir* **2003**, *19*, 6465–6473.
(91) Reynolds, A. J.; Haines, A. H.; Russell, D. A. *Langmuir* **2006**, *22*, 1156–1163.
(92) Natarajan, A.; Xiong, C. Y.; Gruettner, C.; DeNardo, G. L.; DeNardo, S. J. *Cancer Biother. Radiopharm.* **2008**, *23*, 82–91.
(93) Jule, E.; Nagasaki, Y.; Kataoka, K. *Bioconjugate Chem.* **2003**, *14*, 177–186.
(94) Dawson, R. M.; Alderton, M. R.; Wells, D.; Hartley, P. G. *J. Appl. Toxicol.* **2006**, *26*, 247–252.
(95) Yang, H.; Kao, W. J. *Int. J. Nanomed.* **2007**, *2*, 89–99.
(96) Vitte, J.; Benoliel, A. M.; Eymeric, P.; Bongrand, P.; Pierres, A. *Biophys. J.* **2004**, *86*, 4059–4074.
(97) Rinker, K. D.; Prabhakar, V.; Truskey, G. A. *Biophys. J.* **2001**, *80*, 1722–1732.
(98) Levy, R.; Maaloum, M. *Biophys. Chem.* **2005**, *117*, 233–237.
(99) Matrosovich, M. N. *FEBS Lett.* **1989**, *252*, 1–4.
(100) Lanzavecchia, A.; Iezzi, G.; Viola, A. *Cell* **1999**, *96*, 1–4.
(101) Viola, A.; Lanzavecchia, A. *APMIS* **1999**, *107*, 615–623.
(102) Viola, A.; Lanzavecchia, A. *Science* **1996**, *273*, 104–106.
(103) Carter, R. H.; Fearon, D. T. *Science* **1992**, *256*, 105–107.
(104) King, M. R.; Hammer, D. A. *Biophys. J.* **2001**, *81*, 799–813.
(105) King, M. R.; Rodgers, S. D.; Hammer, D. A. *Langmuir* **2001**, *17*, 4139–4143.
(106) Gassmann, P.; Enns, A.; Haier, J. *Onkologie* **2004**, *27*, 577–582.
(107) Kieda, C. *Arch. Immunol. Ther. Exp.* **2003**, *51*, 81–89.
(108) Orr, F. W.; Wang, H. H.; Lafrenie, R. M.; Scherbarth, S.; Nance, D. M. *J. Pathol.* **2000**, *190*, 310–329.
(109) Honn, K. V.; Tang, D. G. *Cancer Metastasis Rev.* **1992**, *11*, 353–375.
(110) Pauli, B. U.; Augustinvoss, H. G.; Elsabban, M. E.; Johnson, R. C.; Hammer, D. A. *Cancer Metastasis Rev.* **1990**, *9*, 175–189.

The fact that multiple numbers of bonds above a threshold typically initiate a biological response, from immune recognition to physicomechanical mechanisms, has important implications for materials design. It suggests that interfacial multivalency, like molecular-level valency, can drive selectivity: cell capture occurs or pathways are initiated only when enough bonds form. These thresholds are sensitive to cellular features beyond the presence or absence of target surface ligands. Therefore, designing materials to exploit interfacial multivalency and to tune adhesion thresholds is one way that greater sophistication (selectivity beyond molecular recognition) can be engineered into new materials.

Biomaterials at the Frontier. A subset of laboratories that study biomaterial interactions also attend to quantitative materials parameters. For instance, the need for multiple cell−cell contacts or multiple cell−matrix contacts is well appreciated; therefore, the concentration of binding sites is a parameter frequently optimized in biomaterial design. In one type of system, fibroblasts were shown to spread on peptide-containing surfaces with RGD spacings on the order of 400 nm.[112] As the surface concentration of RGD is increased, there is an optimal concentration above which the cells bind too tightly and lose their mobility. Below it, cells do not bind well.[113,114] Systematic studies of how the substrate itself influences the optimum peptide surface density are forthcoming. The number of cross-bonds actually formed is also unknown.

Other important surface descriptors are the presentation and surface arrangement of adhesion molecules. The attachment of ligands and receptors directly to a substrate, by adsorption or covalently, often renders the molecules less accessible or weaker in their binding than extending them on polymeric tethers.[115−121] Clustering adhesive functionality (rather than distributing it randomly or uniformly) likewise improves cell-level binding.[95,96,122−125] Separately, the use of a bimodal brush in which the adhesion molecules are placed on long tethers and the remainder of the surface is protected by a lower-molecular-weight brush corona has been proven to improve binding.[115,126−128] As a result, the current thinking tends to be that it is optimal to encourage binding groups to protrude outward from a surface to increase their encounters with molecular targets on approaching surfaces. Maximizing the exposure of binding groups while passivating the remaining surface improves binding and preserves molecular selectivity.

Surfaces That Outperform Individual Adhesion Moieties. Our interest in functional-selective surface design attends to nanoscale adhesive elements placed on a surface but also considers the remainder of the surface to be a material whose properties can be further tuned. The use of adhesive elements to translate molecular-level specificity to the cellular level comprises but one surface design strategy, and in this particular case, we agree with the literature that the remaining surface area should be passivated (for instance, with albumin) to avoid nonspecific attractions to erroneous targets. We do not wish, however, to overlook the opportunity to further control interfacial function through the range, softness, and strength of the repulsion by the portions of the surface that are nonadhesive. In this feature article, we contend that attention to the overall surface design, the nature of the adhesive moieties, and the relative properties of the remainder of the surface can produce surface interactions of substantial sophistication. Most importantly, the features of the adhesive elements, for instance, a solution-phase selectivity index, do not limit the ultimate surface property. This is a very different perspective from the current literature that views the role of the surface as simply preserving the adhesive nature of the binding elements.

As an example, albeit extreme, the current article features new results with adhesive elements or "receptors" that are *not* selective for populations within the suspension objects to which they might be adhered and demonstrates the power of engineering the remaining portion of a surface. We show that, by tuning the range of the repulsion relative to that of attractions localized on adhesive elements, we can switch between the univalent and multivalent adhesion of model cells (spherical particles.) This switching is demonstrated in the context of the capture of flowing particles ("cells") by a functionalized surface, relevant to neutrophil rolling, initial bacterial infection, and cancer metastasis, but is also important in nonbiological applications such as heteroflocculation, colloidal assembly, and lubrication. The system featured here, which was introduced in a short letter,[129] employs adhesive nanoparticles as the attractive elements. This differs from our previous studies employing flat cationic patches.[130−132] The protrusion of the immobilized nanoparticles, as opposed to the flat nature of the previous cationic patches, facilitates the tuning of the binding valency.

The current article demonstrates that, in the multivalent regime but not in the univalent regime, capture is sensitive to other features of the cell surface. That is, cellular-level or microscale selectivity, as opposed to molecular-level specificity, is a consequence of *interfacial* multivalency and cannot be achieved with univalent or single interactions. The latter neglect the opportunity for a type of pattern recognition at the length scales of cellular and particle contact. Thus, we have developed a model system that demonstrates how interfacial (or microscale) multivalency leads to selectivity and that this selectivity does not require discrimination at the molecular level.

The current study therefore provides a quantitative foundation for the development of cell sensing and sorting surfaces. This principle can also form the basis for the selective assembly of particles without the use of expensive and fragile biomolecular fragments. At the same time, the work provides fundamental quantitative insight into the role of adhesion thresholds in

(111) Mundhekar, A. N.; Bullard, D. C.; Kucik, D. F. *Am. J. Physiol.: Cell Physiol.* **2006**, *291*, C130−C137.
(112) Massia, S. P.; Hubbell, J. A. *J. Cell Biol.* **1991**, *114*, 1089–1100.
(113) Gobin, A. S.; West, J. L. *FASEB J.* **2002**, *16*, 751.
(114) Hersel, U.; Dahmen, C.; Kessler, H. *Biomaterials* **2003**, *24*, 4385–4415.
(115) Lin, J. J.; Silas, J. A.; Bermudez, H.; Milam, V. T.; Bates, F. S.; Hammer, D. A. *Langmuir* **2004**, *20*, 5493–5500.
(116) Hern, D. L.; Hubbell, J. A. *J. Biomed. Mater. Res.* **1998**, *39*, 266–276.
(117) Cao, T.; Wang, A. F.; Liang, X. M.; Tang, H. Y.; Auner, G. W.; Salley, S. O.; Ng, K. Y. S. *Biotechnol. Bioeng.* **2007**, *98*, 1109–1122.
(118) Zhu, J. M.; Xue, J.; Guo, Z. W.; Zhang, L. D.; Marchant, R. E. *Bioconjugate Chem.* **2007**, *18*, 1366–1369.
(119) Klenkler, B. J.; Sheardown, H. *Biotechnol. Bioeng.* **2006**, *95*, 1158–1166.
(120) Shu, X. Z.; Ghosh, K.; Liu, Y. C.; Palumbo, F. S.; Luo, Y.; Clark, R. A.; Prestwich, G. D. *J. Biomed. Mater. Res.* **2004**, *68A*, 365–375.
(121) Kim, D. H.; Klibanov, A. L.; Needham, D. *Langmuir* **2000**, *16*, 2808–2817.
(122) Maheshwari, G.; Brown, G.; Lauffenburger, D. A.; Wells, A.; Griffith, L. G. *J. Cell Sci.* **2000**, *113*, 1677–1686.
(123) Koo, L. Y.; Irvine, D. J.; Mayes, A. M.; Lauffenburger, D. A.; Griffith, L. G. *J. Cell Sci.* **2002**, *115*, 1423–1433.
(124) Irvine, D. J.; Mayes, A. M.; Griffith, L. G. *Biomacromolecules* **2001**, *2*, 85–94.
(125) Mart, R. J.; Liem, K. P.; Wang, X.; Webb, S. J. *J. Am. Chem. Soc.* **2006**, *128*, 14462–14463.
(126) Lin, J. J.; Bates, F. S.; Hammer, D. A.; Silas, J. A. *Phys. Rev. Lett.* **2005**, 95.
(127) NopplSimson, D. A.; Needham, D. *Biophys. J.* **1996**, *70*, 1391–1401.
(128) Kenworthy, A. K.; Hristova, K.; Needham, D.; McIntosh, T. J. *Biophys. J.* **1995**, *68*, 1921–1936.
(129) Zhang, J.; Srivastava, S.; Duffadar, R.; Davis, J. M.; Rotello, V. M.; Santore, M. M. *Langmuir* **2008**, *24*, 6404–6408.
(130) Kalasin, S.; Santore, M. M. *Langmuir* **2008**, *24*, 4435–4438.
(131) Santore, M. M.; Kozlova, N. *Langmuir* **2007**, *23*, 4782–4791.
(132) Kozlova, N.; Santore, M. M. *Langmuir* **2006**, *22*, 1135–1142.

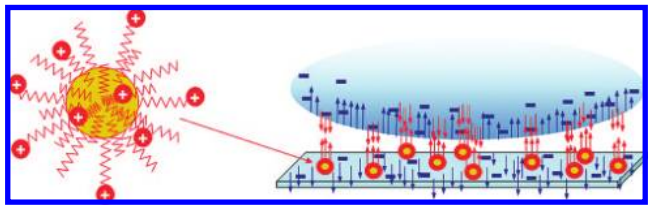

Figure 2. Experimental scheme cationic nanoparticles randomly deposited on negative silica. A negative silica particle approaches.

biological systems, especially those involving surface molecules that bind multiple targets. The ultimate takehome points are (1) that molecular recognition is not necessary for highly selective interfacial interactions, particle adhesion, and assembly and (2) that the design of surfaces to accomplish dynamic function should include a consideration of all regions of the surface, not just the functionalized nanoconstructs that are immobilized.

Design Strategy: Nanoscale Adhesive Elements on Negative Surfaces

The surfaces described here, though nonbiological, bear a semblance to the surfaces of biological cells in that they present nanoscale adhesive elements ("receptors") *randomly arranged* on a substrate whose background is otherwise repulsive (a "glycocalyx" field) toward approaching particles ("cells"). In the current work, these features are electrostatic in nature, though one might more generally produce attractions and repulsions by exploiting any number of different interfacial interactions. Our localization of chemicophysical features rather than biomolecular fragments avoids commitment to a particular ligand−receptor pair and allows access to a broad range of variable space by tuning accessible system parameters. This, in turn, enables the study of fundamental micro- or cellular-scale adhesion behavior.

Gold nanoparticles functionalized with cationic ammonium-terminated ligands,[133] the "receptors," are randomly placed on a negative silica surface, per Figure 2, at modest surface concentrations, of less than 1200/μm^2, corresponding to average spacings of 28 nm or greater. (This range of surface concentrations approaches the relevant range for selectins[134,135] and integrins.[136]) The nanoparticles, including their ligands, have a diameter of 11 nm and protrude, nominally, this distance beyond the silica surface itself, placing cationic groups forward of the supporting substrate.

The large numbers of cationic groups on each nanoparticle (~200, but a fraction of them actually accessible from solution and the rest beneath the nanoparticle) render the nanoattractors multivalent in the sense of the chemist. Using the biologist's definition, however, each nanoparticle could be considered to be an individual receptor. (Because they contain many positive charges, one might think to liken the nanoparticles of the current work and the cationic patches of our prior studies to phospholipid rafts, where the latter concentrate a particular receptor in a small region on a cell surface. We feel, however, that conceptualizing the cationic nanoparticles and adsorbed patches as individual receptors is more appropriate. Receptors clustered together in a raft can still bind each ligand separately. The cluster of cationic charges on our nanoparticles and cationic polyelectrolyte patches cannot bind targets separately and thus do not display the degrees of freedom enjoyed by receptors in a raft. Thus, each nanoparticle or cationic patch should be thought of as a discrete adhesion element.) Pertaining to the chemical multivalency within each gold nanoparticle, it is worth mentioning that with 200 positive charges spread over the surface of an 11 nm sphere there is an average charge spacing of 1.38 nm. This value is greater than the Bjerrum length in water so that minimal nonspecific counterion condensation is expected.

The substrate supporting the cationic nanoparticles is negatively charged silica. When microscale silica particles flow past the compound nanoparticle−silica surface, they experience a complex energy landscape: attractions toward the nanoparticles and repulsions from the rest of the silica substrate. Depending on whether the attractions or repulsions dominate, particles will adhere or escape. One or several nanoparticles may be involved in particle capture, the definition of univalent versus multivalent particle capture used in this work. This article demonstrates how variations in the Debye length allow the system to be tuned between univalent and multivalent particle capture.

This scenario for particle adhesion, in Figure 2, represents a simplification of ligand−receptor binding occurring at the surfaces of biological cells. Whereas the latter require the spatial alignment of complimentary elements across a fluid-filled gap, the cationic nanoparticles in the current study are attracted to any portion of a passing silica particle. This behavior approaches the limit of a densely functionalized flowing particle or cell: the adhesion ability rests entirely with the distribution of receptors on the collecting surface.

Another difference between our system and biological cells is that the current system does not allow for the interfacial restructuring known to occur on the surfaces of cells. Such surface restructuring, triggered by initial adhesion or signaling events, occurs on a timescale of hours, which is much longer than the short contact times relevant to the investigation here. Indeed, the understanding of neutrophil capture and rolling has been substantially advanced by the use of receptor- and ligand-functionalized particles (where the receptors are immobile) interacting with planar surfaces presenting complimentary adhesion molecules.[137−139]

Experimental Detail

Cationic nanoparticles were grown from 7.5 nm gold cores with a shell of approximately 500 ligands. Roughly 200 of these were *N*,*N*,*N*-trimethyl(11-mercaptoundecyl)ammonium chloride side chains, and 300 were 1-mercaptoundecane molecules.[133] With the ligands included, the overall particle diameter was 11 nm, from TEM (measured in the dry state), or 15 nm in solution, measured by dynamic light scattering.[133]

Collecting surfaces were created by random deposition of the cationic nanoparticles onto the silica surfaces of acid-etched microscope slides. This deposition was done by flowing aqueous solutions of the nanoparticles through a slit-shear flow chamber where one of its walls was the acid-etched silica surface.[129] With the mass transfer coefficient of the chamber being well known, the nanoparticle surface density could be precisely controlled by its bulk concentration and flow time. Though this article details the study of silica particle deposition on these surfaces under different ionic conditions, the nanoparticle-containing surfaces were generated using nanoparticles suspended in DI water. We also reran studies using surfaces where the nanoparticles had been deposited from 0.010 M NaCl. Although we were able to obtain higher ultimate

(133) Srivastava, S.; Samanta, B.; Jordan, B. J.; Hong, R.; Xiao, Q.; Tuominen, M. T.; Rotello, V. M. *J. Am. Chem. Soc.* **2007**, *129*, 11776–11780.
(134) Alon, R.; Hammer, D. A.; Springer, T. A. *Nature* **1995**, *374*, 539–542.
(135) Ushiyama, S.; Laue, T. M.; Moore, K. L.; Erickson, H. P.; McEver, R. P. *J. Biol. Chem.* **1993**, *268*, 15229–15237.
(136) Hammer, D. A.; Tirrell, M. *Annu. Rev. Mater. Sci.* **1996**, *26*, 651–691.
(137) Brunk, D. K.; Hammer, D. A. *Biophys. J.* **1997**, *72*, 2820–2833.
(138) Eniola, A. O.; Willcox, P. J.; Hammer, D. A. *Biophys. J.* **2003**, *85*, 2720–2731.
(139) Brunk, D. K.; Goetz, D. J.; Hammer, D. A. *Biophys. J.* **1996**, *71*, 2902–2907.

nanoparticle surface densities at higher ionic strengths, for surfaces having the same nanoparticle densities (but the nanoparticles deposited under different ionic conditions), there was no impact on subsequent silica particle adhesion. Furthermore, we were not able to discern any qualitative impact of the ionic strength during nanoparticle deposition on surface structure, as measured by AFM.

Nanoparticle deposition was tracked in situ using near-Brewster reflectometry, operating in back-reflection mode:[140] A 633 nm He−Ne laser was brought to the silica−water interface from behind, using a triangular prism. The reflected beam was monitored in real time, and data were interpreted using the form for a two-layer model in which the mass of attached gold nanoparticles scaled as the square root of the reflected signal, after background subtraction.[140] Nanoparticle densities were also assessed via AFM after removing the silica flats from the flow chambers and drying them.[129]

Assessing the electrostatic character of planar surfaces, such as our collectors, can be challenging. We therefore employed 1 μm silica particles (from GelTech, Orlando) decorated with small amounts of adherent cationic nanoparticles to approximate the collecting surfaces. Zeta potentials were then measured on a Malvern Zetasizer Nano ZS instrument employing suspensions containing 500 ppm 1 μm silica particles and different amounts of gold nanoparticles. Solution conditions were chosen to match those of the microparticle adhesion studies. The solutions were initially prepared in DI water, and the ionic conditions were subsequently adjusted. Suspensions were stirred overnight to ensure that all nanoparticles had adhered to silica spheres and were sonicated shortly before the measurement. Five separate runs were averaged at each nanoparticle concentration, and data were checked to ensure that only a single sharp peak was present in each sample, indicating a single population.

The capture of flowing microscale silica particles on nanoparticle-bearing surfaces was studied at pH 6.1 and the ionic strength was indicated, employing KH_2PO_4 buffer, with a small amount of NaOH added to adjust the pH. (Buffer dilution in the range of interest did not affect pH). Particles (1 μm) were obtained from GelTech (Orlando), and smaller particles (0.5 μm) were obtained from Fiber Optic Center (New Bedford, MA). Particle suspensions, at a concentration of 1000 ppm, were allowed to flow at a wall shear rate of 20 s^{-1} over the nanoparticle-functionalized surfaces using the same shear chambers employed for nanoparticle deposition. All experiments were conducted in the dilute surface limit: we monitored sufficient numbers of silica particles so that their capture rates were well established; however, this exercise was complete long before the surface became crowded with silica particle. By limiting our study to short times when the surfaces were nearly bare (of microparticles), the interpretation is restricted to particle−collector interactions, with interactions between microparticles avoided.

The adhesion of 1 μm silica particles was monitored using a home-built lateral microscope, where the nanoparticle-containing collecting surface was oriented vertically so that gravity did not affect particle−surface interactions. This instrument mounted the essential elements of a Nikon Diaphot 300 microscope on an optical bench. Data were recorded with standard video equipment, and particle adhesion rates were determined by analyzing the recordings using Image J software. The capture rates of 500 nm silica particles were monitored using the same scanning angle Brewster instrument[140] employed for the nanoparticle deposition. We found the square root of the signal evolution to be proportional to the amount of adherent silica particles as previously detailed.[140] The calibration constant for silica particle capture is not, however, obvious because the silica particles approach the wavelength of light. The instrument was therefore calibrated by examining surfaces containing 500 nm particles on an optical microscope.

Examples and Explanations

Interactions of Solvated Nanoparticles with Silica. Following the typical route of characterizing the solution-phase binding of the adhesive elements before their attachment to a substrate, this section considers the binding of cationic nanoparticles from solution onto silica surfaces.

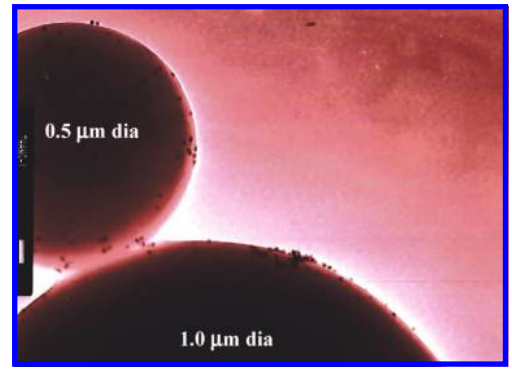

Figure 3. TEM micrograph showing 11 nm gold particles adhering to both 0.5 and 1.0 μm silica particles. The scale bar on the left is 50 nm.

Figure 3 shows a TEM micrograph of two differently sized silica particles with adherent 11 nm nanoparticles. This image was obtained from a suspension containing both 1 and 0.5 μm silica spheres, to which the nanoparticles had been added. Sufficient time was allowed for all of the nanoparticles to adhere to the silica spheres before preparing the dry specimen for TEM. Control images obtained at short times revealed free nanoparticles on the TEM grid. In Figure 3, the nanoparticles were present only on silica spheres, ensuring that their binding occurred before sample preparation for TEM. Thus, Figure 3 confirms, albeit qualitatively, the expectations that the adhesive cationic elements show no solution-phase preference for either size silica particle. The electrostatic and van der Waals forces drive strong nonselective attractions. Figure 3 also provides a useful perspective on the relative sizes of the objects involved.

Before moving on to microparticle interactions, we further explore the binding of the nanoparticles to planar surfaces. This places a lower bound on the nanoparticle binding kinetics, provides an assessment of nanoparticle surface density on the planar surfaces, and demonstrates how collecting surfaces are fabricated. Figure 4 presents nanoparticle deposition data for nanoparticle solutions flowing over acid-etched microscope slides in a slit-shear chamber.[140,141] The effect of bulk solution concentration is highlighted in part A. For each run, the nanoparticle accumulation is linear in time, and the deposition rate increases linearly with bulk solution concentration in the inset. For slit-shear flow chambers of the geometry employed here, the steady-state mass-transport-limited particle deposition rate, $d\Gamma/dt$, is described by the Leveque equation:[142]

$$\frac{d\Gamma}{dt} = \frac{1}{\Gamma(4/3)9^{1/3}}\left(\frac{\gamma}{DL}\right)^{1/3} DC \qquad (1)$$

Here, C is the bulk solution nanoparticle concentration, γ is the wall shear rate, L is the distance from the entrance of the chamber to the point of observation, and on the right-hand side of eq 1, and only here, $\Gamma(4/3)$ is the gamma function evaluated at an argument of 4/3. D is the bulk solution diffusion coefficient of the nanoparticles, 3.3×10^{-8} cm^2/s, measured by dynamic light scattering.

The nanoparticle deposition rate, calculated from eq 1, is in good quantitative agreement with the observed rates. The adherence of the nanoparticle deposition to these transport-limited

(140) Fu, Z. G.; Santore, M. M. *Colloids Surf., A* **1998**, *135*, 63–75.

(141) Shibata, C. T.; Lenhoff, A. M. *J. Colloid Interface Sci.* **1992**, *148*, 485–507.

(142) Leveque, M. A. *Ann. Mines* **1928**, *13*, 284.

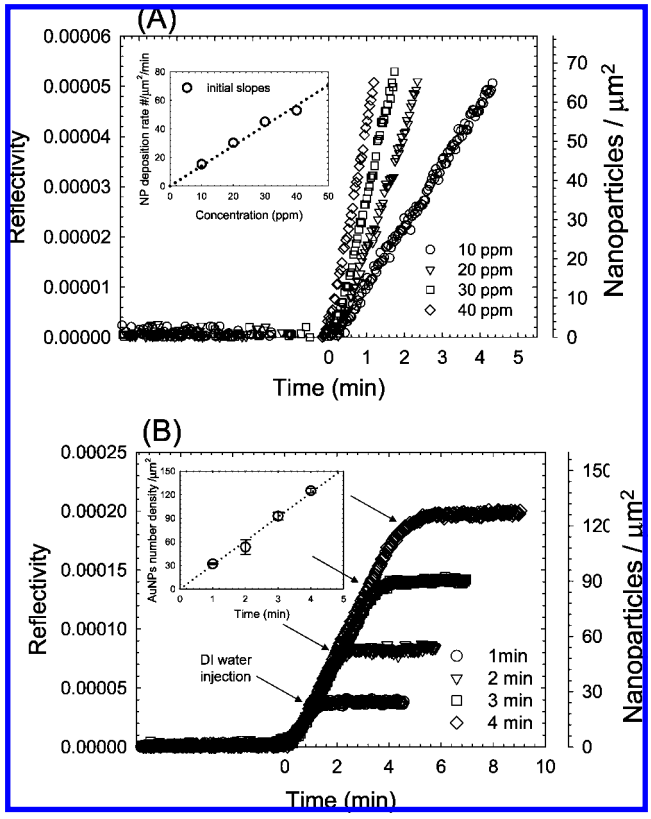

Figure 4. (A) Representative reflectometry data for the deposition of cationic nanoparticles from DI water on acid-etched microscope slides at a wall shear rate of $10s^{-1}$ for different nanoparticle concentrations. The inset shows how the deposition rate depends on concentration. (B) Procedure to deposit controlled amounts of nanoparticles involving the reinjection of DI water after a period of time. Representative data are for a nanoparticle concentration of 20 ppm in DI water and a wall shear rate of 10 s^{-1}. The inset shows the ultimate nanoparticle density as a function of flow time. Part B has been reproduced from ref 129.

kinetics reinforces our expectations for strong attractions between the nanoparticles and the silica flat arising from both electrostatic and van der Waals attractions. This adherence is also consistent with our observations that (1) the nanoparticle placement on the silica appears to be random: there is no evidence for lateral diffusion of the nanoparticles on the silica flat prior to their final attachment[129] and (2) the nanoparticles are retained on the silica surface under a variety of conditions including drying, sonication, and exposure to organic solvents, and (3) the dry nanoparticle heights on silica as measured by AFM are slightly smaller than the TEM particle diameter: the ligand shell likely deforms by 1 to 2 nm to increase contact with the substrate and bring the gold core closer to the silica (driven by strong van der Waals attractions.) It is worth noting that this reduction in the nanoparticle height relative to the dry TEM particle diameter cannot be explained by the surface roughness of the microscope slide, which is 0.3−0.5 nm.

Figure 4B presents a series of nanoparticle deposition runs, interrupted at different times by the reinjection of flowing DI water to demonstrate the production of collecting surfaces. When water is injected, nanoparticle accumulation halts, and the reflectometry signal becomes flat, indicating particle retention on each surface. By precisely timing the duration of the nanoparticle flow, the density of deposited nanoparticles could be tuned at a targeted level, as shown in the inset.

To summarize, Figure 4 makes two points. First, it demonstrates how we fabricate heterogeneous collecting surfaces with precise control over the average nanoparticle density. To date, we have

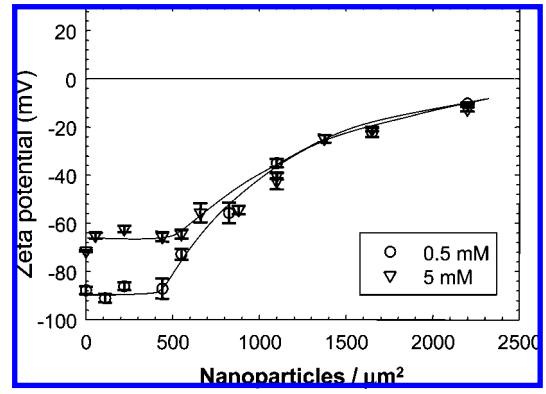

Figure 5. Zeta potential of 1 μm silica particles containing different amounts of adsorbed cationic nanoparticles. The curves guide the eye but have no quantitative significance.

produced surfaces with as few as 9 nanoparticles/μm^2 and as many as 3000 nanoparticles/μm^2. The ability to control the density of surface functionality relies largely on the bulk solution concentration of nanoparticles employed. This method has been applied to a variety of adhesion constructs and molecules, ranging from cationic polymers to proteins.[130−132,143,144] Second, the nanoparticles, on which we focus here always deposit at the transport-limit rate. In the context of the state space of descriptors of adhesion moieties, the forward binding rate between solvated cationic nanoparticles and a silica surface is fundamentally fast. Connecting to literature on receptor physics, it is known, for instance, that neutrophil rolling on the endothelium requires a fast forward binding constant[68,69,136] such as that seen with the cationic nanoparticles, but rolling also depends on the dissociation rate constant. The latter is not addressed here.

Energy Landscape of a Heterogeneous Surface. It is worthwhile to consider how the average properties of the composite surfaces, cationic nanoparticles on a silica support, vary with nanoparticle loading. Information such as the surface or zeta potential is useful in aiding the interpretation of the particle adhesion studies in the following sections. Quantification of the zeta potential also facilitates a comparison between our system and other charge-heterogeneous systems (mineral, polymer, and biological) where more detailed surface characterization is not forthcoming.

Figure 5 shows the influence of cationic nanoparticles on the zeta potential of the composite surface at pH 6.1 in the two buffer ionic strengths studied for microparticle capture. These results were obtained by employing 1 μm silica spheres as models for the planar collecting surfaces. A 500 ppm suspension of silica particles in DI water was mixed with small amounts of nanoparticle solution and agitated vigorously for ~2 h. The ionic strength was then adjusted, and the solutions stirred overnight to ensure that all of the nanoparticles adhered to the silica spheres. TEM was performed on samples to ensure that all the nanoparticles were associated with microparticles, and indeed, for short times we were able to identify nanoparticles that had been free in solution prior to their drying on the microscopy grid. Depending on the concentration of nanoparticles added, the silica spheres were not necessarily stable singlets. Therefore, suspensions were sonicated prior to measurement of the zeta potential to redisperse the microspheres. Sonication did not impact nanoparticle adhesion, as was confirmed separately via AFM, on nanoparticle-containing flats.

(143) Toscano, A.; Santore, M. M. *Langmuir* **2006**, *22*, 2588–2597.
(144) Santore, M. M.; Wertz, C. F. *Langmuir* **2005**, *21*, 10172–10178.

In Figure 5, the zeta potential of the composite interface decreases in magnitude, becoming less negative with increasing addition of cationic nanoparticles. For nanoparticle concentrations in the range 0−450 particles/μm^2, the influence of the nanoparticles on the zeta potential is negligible. Below about 2500 nanparticles/μm^2, which is inclusive of the conditions of interest for silica particle capture, the average character of these surfaces is net negative. At higher nanoparticle surface densities beyond the range shown here, the zeta potentials were positive and ultimately reached a plateau at the +20 mV value of the cationic nanoparticles themselves.

As will be shown in the next sections, interesting microparticle adhesion can occur with particle concentrations well below 450/μm^2, in the regime where the zeta potential is indistinguishable from that of bare silica. This finding is in consistent with literature that implicates charge heterogeneity in bacterial adhesion[145−148] and microparticle flocculation[149−151] between objects that are substantially net negative and where the presence of charged clusters is difficult to detect.

Silica Particle Capture: Tuning Valency with Ionic Strength. The interaction of silica microspheres with nanoparticle-functionalized surfaces was assessed by quantifying the rate at which flowing silica particles were captured by heterogeneous surfaces in a slit-shear flow cell. Studies were confined to times sufficiently short that the surfaces did not become crowded with microparticles. Thus, the presence of some microparticles on the surface did not influence the rate at which additional particles were captured, as confirmed by the linearity of the deposition curves.

By way of example, Figure 6 shows kinetic data for the capture of flowing silica microparticles (20 s^{-1} wall shear rate) on collecting surfaces containing different numbers of cationic nanoparticles. Part A shows the capture of 1 μm particles from a 1000 ppm suspension in 0.005 M pH 6.1 buffer, recorded on video and analyzed with image-processing software whereas part B shows the capture of 0.5 μm particles at the same bulk suspension concentration measured by near-Brewster reflectometry. In several runs, lines indicate how the particle capture rate was determined.

Figure 7 summarizes the silica particle capture rates for different silica particle sizes and ionic conditions as a function of the density of cationic nanoparticles on the surface. At an ionic strength of 0.005 M, which corresponds to a Debye length of 4.24 nm (smaller than the nanoparticles), both data sets for the 1 and 0.5 μm particles pass through the origin in the limit of low nanoparticle density on the collector. This indicates that there is always a finite capture rate for silica particles as long as there are some gold nanoparticles on the surface. Taken further, this argument implies that even with only one nanoparticle on the collecting surface one microparticle (either 0.5 or 1.0 μm in size) would ultimately be captured, albeit very slowly. Thus, the passing of the data through the origin defines the univalent particle capture regime.

To clarify our definition, in the univalent regime, that is, with a Debye length of 4.24 nm, only one immobilized nanoparticle

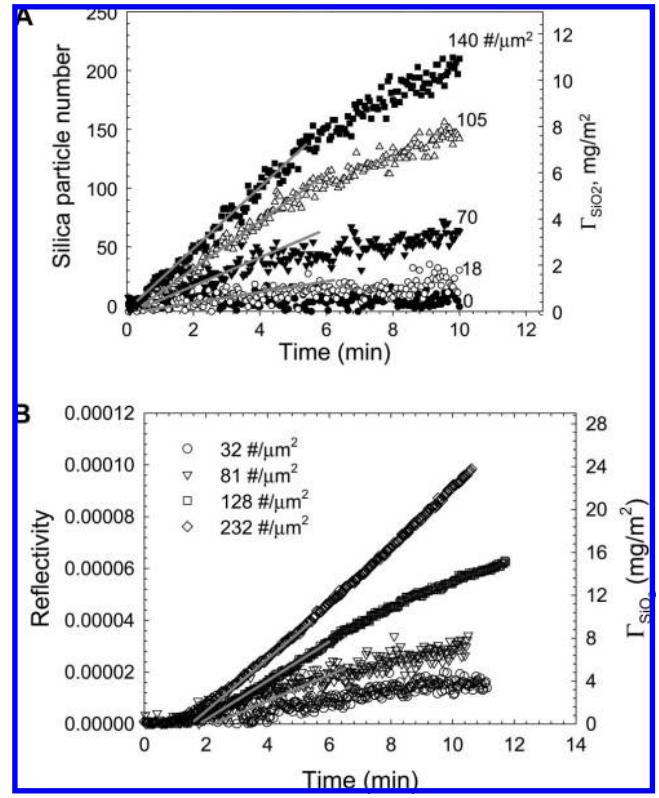

Figure 6. Raw data for 1 μm silica particle accumulation on surfaces with different densities of gold nanoparticles, with the latter indicated on the data labels. The ionic strength is 0.005 M. Gray lines indicate how deposition rates were estimated. Raw reflectometry data for 0.5 μm silica particle accumulation on surfaces with different densities of gold nanoparticles, with the latter indicated on the data labels. The ionic strength is 0.005 M. Gray lines indicate how deposition rates were estimated.

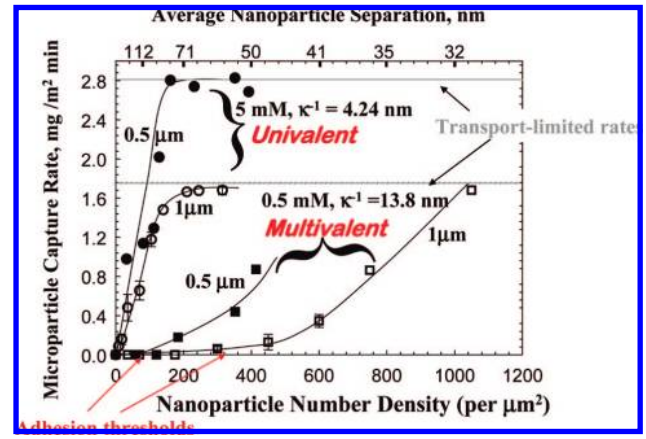

Figure 7. Adhesion rates of 1 and 0.5 μm silica particles on surfaces containing different densities of gold nanoparticles.

is *necessary* for the capture of each microparticle. However, depending on the density of nanoparticles on the collecting surface, more nanoparticles may be involved than the single one actually required.

In Figure 7, in the univalent capture regime (within ~4 nm Debye length) the 0.5 μm particles adhere slightly more quickly to the surface than do the 1 μm particles as the data approach the origin. This slight difference is likely due to the faster diffusivities of the smaller particles. We believe that the fundamental attractions of the immobilized nanoparticles to either 0.5 or 1 μm particles are the same in the univalent regime and

(145) Jones, J. F.; Feick, J. D.; Imoudu, D.; Chukwumah, N.; Vigeant, M.; Velegol, D. *Appl. Environ. Microbiol.* **2003**, *69*, 6515–6519.
(146) Faille, C.; Membre, J. M.; Tissier, J. P.; Bellon-Fontaine, M. N.; Carpentier, B.; Laroche, M. A.; Benezech, T. *Biofouling* **2000**, *15*, 261–274.
(147) Johnson, P. R.; Sun, N.; Elimelech, M. *Environ. Sci. Technol.* **1996**, *30*, 3284–3293.
(148) Ryan, J. N.; Elimelech, M. *Colloids Surf., A* **1996**, *107*, 1–56.
(149) Holtzer, G. L.; Velegol, D. *Langmuir* **2003**, *19*, 4090–4095.
(150) Velegol, D.; Feick, J. D. *Langmuir* **2003**, *19*, 4592–4596.
(151) Jones, J. F.; Holtzer, G. L.; Snyder, C.; Yake, A. M.; Velegol, D. *Colloids Surf., A* **2005**, *267*, 79–85.

that the observed difference comes down to particle dynamics. Indeed, with densities of nanoparticles on the collecting surface above ~200 nanoparticles/μm^2, the microparticle capture rates becomes transport-limited, as indicated by the gray lines. These maximum transport-limited capture rates for the microparticles were calculated via eq 1, with the diffusivities of the 0.5 and 1.0 μm particles following from the Stokes−Einstein equation: 9.8×10^{-9} and 4.9×10^{-9} cm^2/s, respectively. The observed capture rates approach these limits as the surface is made more adhesive.

The univalent capture regime is defined by the ability of single adhesive elements to capture flowing silica microparticles. Because the adhesive nanoparticles (in solution) are not selective for a particular silica sphere, nanoparticle−silica sphere adhesion in the univalent regime is similar to that in free solution as described in the previous section. Nanoparticle immobilization on a silica flat has little effect on the binding of silica microspheres. Indeed, once microspheres are captured by individual nanoparticles, for instance, on surfaces with only 9 nanoparticles/μm^2, they cannot be removed by increased flow up to 1100 s^{-1},[129] which corresponds to a shear force of 9 pN on the 1 μm microspheres. The attractive electrostatic and van der Waals forces between an immobilized nanoparticle and the adherent silica sphere are orders of magnitude stronger than the hydrodynamics. The silica spheres are, however, released when the ionic strength is decreased so that the Debye length approaches the nanoparticle dimensions.[129] The increased Debye length shifts the system into the multivalent regime, as discussed next, so that the single nanoparticle that originally held each microsphere is no longer sufficient to keep it bound to the surface.

Figure 7 includes the impact of ionic strength on particle capture: the rightmost data sets for the two silica particle sizes were obtained with more dilute buffer, 0.0005 M, with a corresponding Debye length of 13.8 nm. Now the electrostatic length scale exceeds the nanoparticle dimensions, making their protrusion from the surface unimportant. Here, neither data set for either particle size approaches the origin. Instead, two adhesion thresholds, highlighted by the arrows, are seen. For collecting surfaces whose nanoparticle densities fall below the thresholds, microparticle capture is not possible. These surfaces below the thresholds contain nanoparticles, and if under these conditions individual nanoparticles were capable of adhering single microparticles, then a finite particle capture rate would be expected. Therefore, the presence of an adhesion threshold indicates that multiple nanoparticles must be engaged in the adhesion of single nanoparticles, defining the regime of multivalent particle capture. At the adhesion threshold for a particular microparticle type, a minimum number of nanoparticles are engaged in microparticle capture. At nanoparticle concentrations above each threshold, a greater number of nanoparticles may be involved.

In the multivalent regime, the net effective contribution of each nanoparticle to the capture of a microparticle must be less than it is in the univalent regime. Otherwise, again, a single nanoparticle would be able to capture and hold a silica microparticle. Figure 8 illustrates how this occurs: At ionic strengths of 0.005 M with a Debye length of 4.24 nm, the electrostatic attraction between the nanoparticles and silica microspheres is virtually uninfluenced by the negative silica support. When the microsphere contacts a nanoparticle, the repulsive support is more than a Debye length away. As the Debye length is made to exceed the cationic nanoparticle size, however, the protrusion of the nanoparticles forward of the negative flat becomes less important. The attractions from the nanoparticles and repulsions from the silica support act more nearly equally (say, per unit surface charge) on a silica microsphere, setting up a competition between attractions and repulsions. Thus, silica particle capture becomes multivalent.

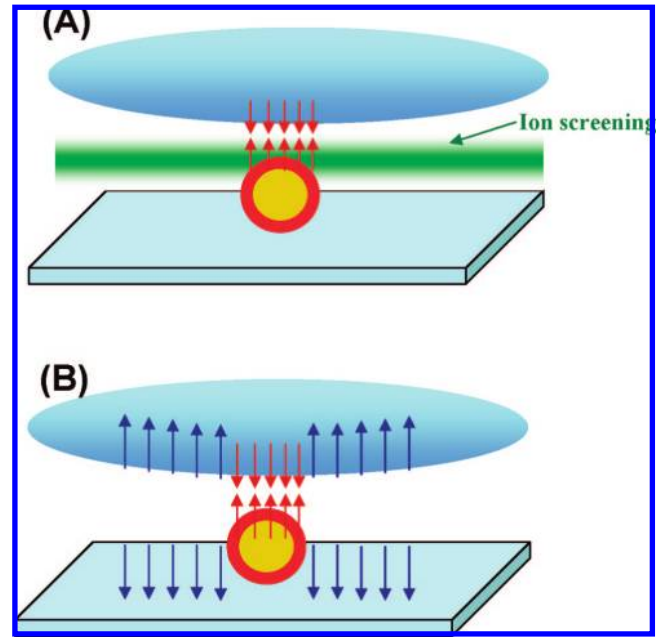

Figure 8. Valency is tuned with the repulsive field. (A) In the univalent regime, at high ionic strength (small Debye lengths), repulsive interactions between the silica sphere and the planar substrate are screened. The attractions between the silica sphere and the nanoparticle persist because the nanoparticle protrudes beyond a Debye length from the surface. (B) In the multivalent regime at low ionic strength (large Debye lengths), the repulsions between the sphere and the substrate compete with the attractions between the sphere and the nanoparticle. Each adhesive element becomes insufficient for particle capture.

This effect of ionic strength essentially tunes the binding strength of the individual nanoparticles by altering the importance of the background field. The binding character shifts between univalent and multivalent because with weak effective binding energy more bonds are needed to capture particles. This multivalency alone, however, is insufficient to produce interfacial selectivity. As discussed below, there is a second effect of ionic strength related to the particle size sensitivity of the threshold, which produces selectivity in this system.

Multivalent Regime: From Thresholds to Selectivity. An important consequence of multivalent particle capture is that adhesion thresholds are particle-dependent, sensitive to differences in local curvature (or size) and other properties, such as particle modulus or the compressibility of a steric layer. Therefore, if one considers two different particle types, each with its own adhesion threshold, the surface compositions between the two thresholds will adhere one particle type and reject the other, providing a nearly perfect separation. Thus, micron-scale specificity is achieved without selectivity on the molecular level.

The power of particle-dependent thresholds is illustrated in Figure 9. Part A reproduces, for the sake of clarity, the silica particle capture data from Figure 7 at low ionic strength, 0.5 mM, now identifying, (B), a collecting surface composition that should discriminate large and small particles. Also chosen is a control surface composition, (C), that should not discriminate the large and small particles beyond the differences in their transport rates. In the subsequent experiments, a particle mixture, having a weight ratio of 3:1 for 1 μm relative to 0.5 μm particles, was flowed over both surfaces in Figure 9B. On the selective surface, only the 0.5 μm particles adhere from the mixture (despite the fact that it contained 3 times as much, by weight, of the 1.0 μm particles), because its nanoparticle surface concentration was

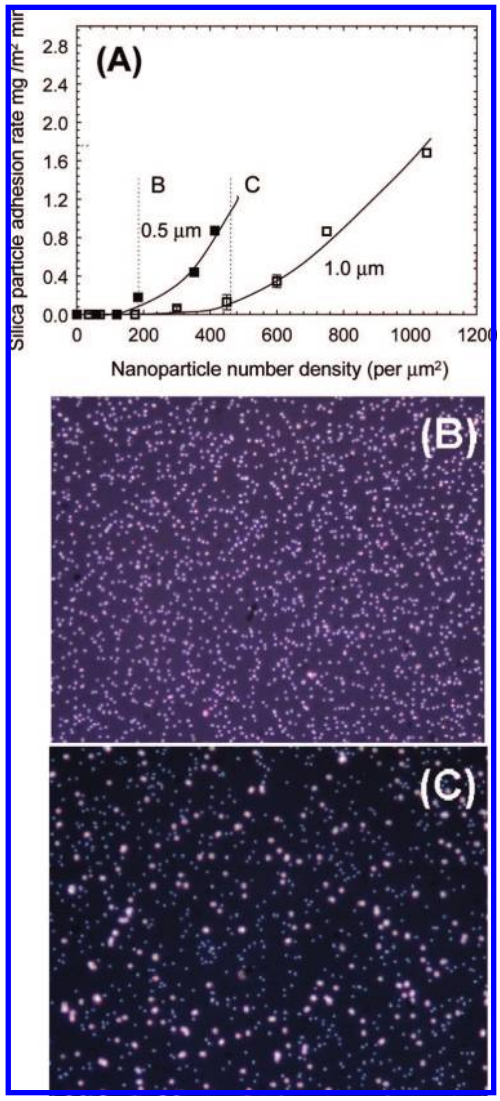

Figure 9. (A) Choice of selective collector and control collector, for an ionic strength of 0.005 M. (B) Selective collector after exposure to a mixture of 0.5 and 1.0 μm particles. (C) Control collector after exposure to a mixture of 0.5 and 1.0 μm particles.

below the threshold for the capture of 1 μm particles, but above the threshold for capture of 0.5 μm particles. The selectivity of this surface for the smaller particles and near perfect rejection of 1 μm particles is striking. The control surface shows that both types of particles adhere from the mixture in the expected proportions, above both thresholds.

Figure 10 illustrates, by way of comparison, particle capture from a mixture in the univalent regime with a Debye length of 4.24 nm, which is smaller than the nanoparticle height. To ensure that particle capture would be by single nanoparticles, the collector surface composition in part A was chosen to be 9 nanoparticles/μm^2. When the same particle mixture from Figure 9, now at an ionic strength of 5 mM, was flowed over this collecting surface, both particle sizes were seen to adhere in part B. Any differences between the surface composition and the bulk solution composition reflect differences in the transport dynamics of the particle, not surface selectivity. Indeed, the lack of adhesion thresholds in the univalent regime is consistent with the observed lack of selectivity here.

Figures 9 and 10, taken together, illustrate the importance of multivalency to the ability of whole interfaces to discriminate approaching objects. Near-perfect specificity for adhering small

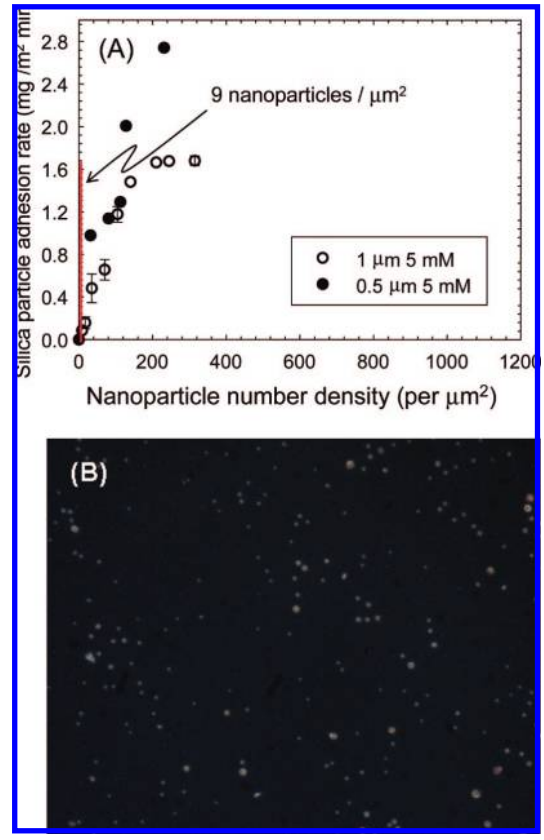

Figure 10. (A) Composition of test surface shown in the univalent regime. (B) Optical micrographs of 1 and 0.5 μm silica particles adhering from a mixture to the surface containing 9 nanoparticles/μm^2 at an ionic strength of 5 mM.

particles and rejecting large ones is found only in the multivalent regime, at low ionic strengths and large Debye lengths. It is not possible to choose a surface composition in the univalent regime (with higher ionic strengths and smaller Debye lengths) that discriminates silica spheres. This is the case because the nanoparticles act, in the multivalent regime, forward of the repulsive background surface, approximating their strong non-discriminating adhesion in free solution.

The relationship between multivalency and selectivity stems from the sensitivity of the adhesion threshold to particle features. The mechanism by which this occurs for the interactions of silica particles with negative surfaces presenting cationic elements is shown in Figure 11 and follows the discussion presented in our papers on flat cationic patches.[130−132] The selectivity is derived from the interplay of several factors: (1) the random or disordered nature of the arrangement of adhesive surface elements, (2) the net or average repulsive character of the particle−surface interactions (i.e., the collecting surfaces are net negative, as indicated by their zeta potentials in Figure 3), and (3) the finite effective contact area or "zone of influence" between a silica particle and the collecting surface. Because the surface is net repulsive, particle capture requires a spatial fluctuation, or hot spot in which the local concentration of adhesive elements exceeds the average surface concentration, where the latter is represented on the x axis of Figure 7.

In Figure 11, the zone of influence is defined quantitatively as the collector area that exerts an electrostatic force on the particle. As shown in Figure 11B,[152] for a particle positioned above the surface, the maximum interaction occurs toward the

(152) Duffadar, R. Ph.D. Thesis, Univesity of Massachusetts, 2008.

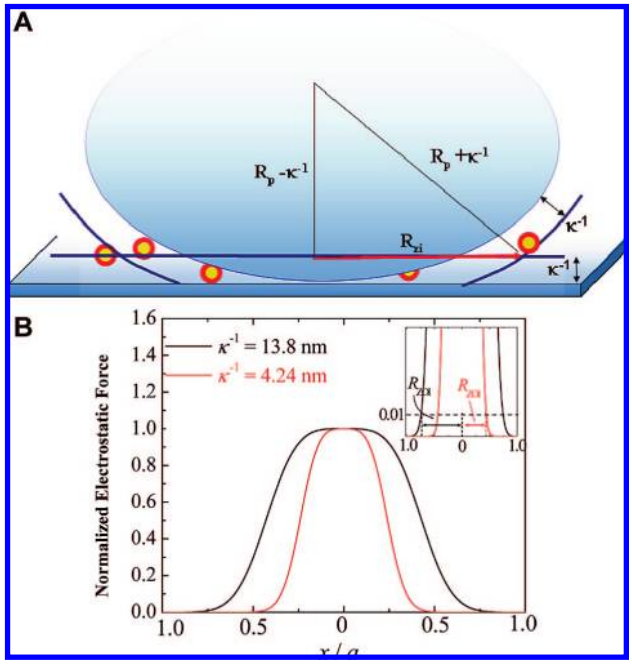

Figure 11. (A) Zone of influence increasing with increasing Debye length. (B) Calculated electrostatic forces as a function of distance from the midaxis. The inset shows a closeup where the zone of influence is chosen to correspond to 99% of the total force (from ref 152).

Table 1. Radius of the Zone of Influence, R_{zi}

particle diameter, μm	R_{zi}, nm for κ^{-1} = 4.24 nm	R_{zi}, nm for κ^{-1} = 13.8 nm
0.2	41	72
0.5	65	114
1.0	92	161
2.0	130	228

particle's middle axis (the line perpendicular to the planar surface that passes through the particle's center) where its surface is closest to the collector. For interactions dominated by electrostatics, the distinction between interacting and not interacting is defined by the Debye length, hence the zone of influence in Figure 11 results from the overlap between the Debye shell around the particle and a Debye cushion over the collector and is $R_{zi} = 2(\kappa^{-1}R_p)^{1/2}$. Thus, the geometrical argument for the zone of influence attributes similar importance to the particle radius and Debye length (which scales as $I^{-1/2}$.) Duffadar has shown that this geometrical description of the zone of influence accounts for 99% of the electrostatic interaction for a variety of particle sizes and ionic strengths.[152,153]

Typical sizes for the zone of influence are shown in Table 1. Of note is the fact that this length scale is much smaller than that of the microspheres and approaches the spacing of the nanoparticles themselves. The zone of influence is, however, quite sensitive to the particle curvature, with R_{zi} increasing by more than 40% as the particle size is doubled. Returning to the requirement of an above-average concentration of adhesive elements for particle capture, the elevated nanoparticle concentration must occur within a surface region that is the size of the zone of influence. There is a greater probability of finding such a hot spot in systems where the zone of influence is small (small particles, high ionic strength) because the spatial fluctuation itself need not be large nor involve a large number of adhesive elements. Conversely, in systems with large zones of influence (large particles and low ionic strengths) particles tend to sample the more average (repulsive) surface character, and hence a larger hot spot is needed for particle capture. Thus, the threshold is shifted to the right for larger particles (and lower ionic strength) within the multivalent regime.

To summarize the mechanism for interfacial specificity in the multivalent regime, different thresholds for different particle sizes are determined by the probability of an approaching particle finding a surface region with a sizable hot spot. This probability depends on the random distribution of adhesive elements convoluted with the contact area, where the latter is sensitive to particle character. In the examples presented here, nearly perfect discrimination based on particle size was illustrated; however, it is worth noting that we have previously documented the ability to discriminate particles on the basis of curvature: aggregates of small spheres, though larger in overall size, are more adhesive on patchy collectors than smooth particles of moderate size. Indeed, the size of the zone of influence is actually sensitive to the local radius of curvature, which happens to be equal to the particle diameter in the current case of spheres.[131]

Other particle characteristics, besides curvature or shape, will influence the contact area and can form the basis for particle discrimination. Properties such as a particle's background charge (analogous to the silica charge here), bulk modulus, or even the compressibility of a cellular glycocalyx and the chain length on which receptors are extended can substantially influence the contact area. As Table 1 demonstrates, a very small change, on the order of nanometers in the Debye length, produces substantial differences in the zone of influence, leading to particle discrimination. We expect that nanometer-scale differences in the deformability of cells or of the thickness of the gyclocalyx relative to the positioning of receptors will produce a similar effect.

Selectivity of Classical Colloidal Systems. It is worth mentioning that selective particle interactions, at the level of the interface or whole particle, have long been a topic of interest in classical colloids research, driven by the need for separations in mineral flocculation,[154−156] wastewater treatment,[157−160] and papermaking.[157,161] Indeed, selective flocculation is practiced in important industrial processes.

The use of polymers and surfactants as selective flocculants has been documented for decades. Most of this literature focuses on the ability of the adsorbing polymer to discriminate between particles of different surface character,[154−157,161−163] a mechanism that is equivalent to the molecular-recognition approach, albeit not as highly selective. We note that in such applications if the flocculant is added at levels insufficient to saturate the particle surfaces then the interfacial selectivity−multivalency approach described here likely contributes to the separation process. This contribution can be favorable or unfavorable, depending on the particular processing goal. The literature on selective flocculation

(153) Duffadar, R. D.; Davis, J. M. *J. Colloid Interface Sci.* **2008**, *326*, 18–27.

(154) Sresty, G. C.; Somasundaran, P. *Int. J. Miner. Process.* **1980**, *6*, 303–320.

(155) Laskowski, J. S.; Qi, L.; Bolin, N. J. *Int. J. Miner. Process.* **1991**, *33*, 223–234.

(156) Weissenborn, P. K.; Warren, L. J.; Dunn, J. G. *Colloids Surf., A* **1995**, *99*, 11–27.

(157) Salt, D. E.; Hay, S.; Thomas, O. R. T.; Hoare, M.; Dunnill, P. *Enzyme Microb. Technol.* **1995**, *17*, 107–113.

(158) Helander, I. M.; Alakomi, H. L.; LatvaKala, K.; Koski, P. *Microbiology (Reading U.K.)* **1997**, *143*, 3193–3199.

(159) Agerkvist, I. *Colloids Surf.* **1992**, *69*, 173–187.

(160) Henry, K. L.; Davis, R. H.; Taylor, A. L. *Biotechnol. Prog.* **1990**, *6*, 7–12.

(161) Dickinson, E.; Eriksson, L. *Adv. Colloid Interface Sci.* **1991**, *34*, 1–29.

(162) Hocking, M. B.; Klimchuk, K. A.; Lowen, S. *J. Macromol. Sci., Rev. Macromol. Chem. Phys.* **1999**, *C39*, 177–203.

(163) Swerin, A.; Odberg, L.; Wagberg, L. *Colloids Surf., A* **1996**, *113*, 25–38.

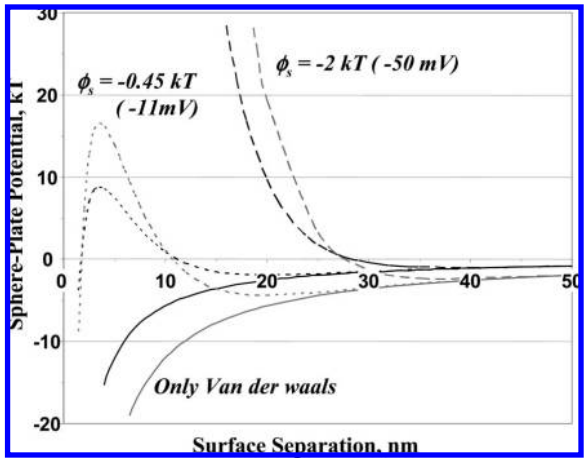

Figure 12. DLVO calculations comparing sphere−plate interactions for 1.0 (gray) and 0.5 (black) μm spheres.

does not, however, make the connection between valency and selectivity as we do here, though it goes as far as appreciating curvature-sensitive contact areas in a few cases.[161,164,165]

It is also worth pointing out that the fundamental colloid literature has long described the size or curvature effect on interactions between entirely homogeneous surfaces. Classical DLVO theory contains different particle-size scaling for the van der Waals and electrostatic forces.[166] As an example, Figure 12 illustrates DLVO calculations for sphere−plate interactions involving 0.5 versus 1.0 μm spheres. One set of parameters approximates silica as an entirely homogeneous surface: a surface potential of about −50 mV or $-2kT$ and a nonretarded Hamaker constant that is electrostatically screened[167] ($A_{\text{nonscreened}} = 1.57kT$ and $0.62kT$). By way of comparison, the pure van der Waals term is plotted for the two particle sizes, and a second lower surface potential is also shown. For a surface potential of $-2kT$, there is only a weak secondary minimum that is slightly more attractive for the larger particles. However, with a reduced surface potential, the energy barrier for the 1 μm spheres is larger than that for a 0.5 μm sphere. The smaller particles are indeed more adhesive for the plate, even in the mean-field sense.

Although DLVO theory predicts that small particles can be stickier than large ones, this result differs substantially from our examples with the nanoparticle-containing surfaces. With DLVO, modest differences in the energy barrier will ultimately allow both particle sizes to adhere to the plate, but at different rates. This produces selectivity but not the nearly perfect specificity in Figure 9.

Summary and Perspective

This work has demonstrated how surfaces containing discrete randomly placed binding elements can be designed to control the *interfacial* valency for microparticle binding, that is, the numbers of adhesive elements necessary to bind microscale objects. A key point is that the nanoscale adhesion elements themselves need not be selective for microscale objects. Multivalency at the interfacial scale alone, when properly tuned, produces nearly perfect selectivity. As an example, we showed the binding of 0.5 μm silica particles and the complete rejection of micrometer-sized particles.

This article presented a new system to develop the interfacial multivalency concept: a negative silica surface containing 11 nm cationic nanoparticles that protruded roughly this distance from the silica substrate. The main silica flat repelled approaching negative microparticles whereas the cationic nanoparticles were attractive. By tuning the ionic strength to manipulate the Debye length relative to the diameter of the immobilized nanoparticles, the valency for particle capture was adjusted to between univalent and multivalent. At small Debye lengths, the electrostatic repulsion between the silica flat and the approaching microspheres was screened, leaving the protruding cationic nanoparticles to bind flowing silica spheres strongly. Indeed, single surface-immobilized nanoparticles were able to capture and hold 1 μm silica spheres in a strong shear field with forces of 9 pN or more as a result of the relative importance of electrostatics compared with hydrodynamics. The microparticles could be released only by reducing the ionic strength. Conversely, when the Debye length was greater than the size of the immobilized nanoparticles, the nanoparticle attractions needed to overcome the electrostatic repulsion between the planar substrate and the approaching microsphere. This effectively weakened the binding energy per nanoparticle and produced multivalent binding. Here, there was an adhesion threshold: microparticle capture by collecting surfaces was observed only above a critical loading of nanoparticles on the collector.

Because the threshold is sensitive to the nature of the microparticles, it is possible, in the multivalent regime but not in the univalent regime, to selectively adhere populations of particles with great discrimination. By way of example, we demonstrated the adhesion of 0.5 μm silica spheres whereas 1 μm particles were completely rejected by a collecting surface. We also demonstrated why this was not possible in the univalent regime: when one immobilized nanoparticle is sufficient for microparticle binding, the character of the binding element dominates other interfacial considerations, and the nonselective (in this case) solution-phase binding is recovered.

The mechanism by which selectivity arises in the multivalent regime involves the random distribution of adhesive nanoelements on the repulsive collector but also critically depends on the contact area between the collector and the target. For interactions dominated by electrostatics, this behavior is governed by the Debye length, but it also is a strong function of the local curvature of the objects themselves. Because more sharply curved objects (such as small spheres) have a smaller contact area with planar surfaces, their interactions are more sensitive to surface heterogeneity. In this case, the attractive hot spots caused by the randomness in the nanoparticle surface distribution produce attractions.

In general, any feature that alters the effective contact area can be exploited as a basis for selectivity. Thus the particle modulus, the compressibility of the polymer brush on its surface, and the extension of adhesive groups on tethers are all features that can be discriminated by the interfacial multivalency mechanism. The interactions are also sensitive to general interfacial features such as the surface potential or the strength of the van der Waals forces. Finally, the distribution of receptors on the collecting surface and target surface is sure to be important as well. Just as surface curvature constitutes a means by which more sharply curved objects can bind to hot spots while avoiding the repulsive regions just outside the hot spots, the concentration of molecular targets in rafts would allow biological targets to adhere to a collecting surface most strongly. Thus, for instance, these surfaces

(164) Yiantsios, S. G.; Karabelas, A. J. *J. Colloid Interface Sci.* **1995**, *176*, 74–85.
(165) Tsouris, C.; Scott, T. C. *J. Colloid Interface Sci.* **1995**, *171*, 319–330.
(166) Russel, W. B.; Schowalter, W. R.; Saville, D. A. *Colloidal Dispersions*; Cambridge University Press: Cambridge, U.K., 1989.
(167) Israelachvili, J. *Intermolecular and Surface Forces*, 2nd ed.; Elsevier: Amsterdam, 1992.

will discriminate targets with clustered as opposed to more nearly uniformly distributed biological functionality. Finally, we wish to emphasize that whereas the principle of interfacial multivalency and discrimination was demonstrated here with completely nonselective adhesive elements the same principles would apply to elements that possess molecular specificity. Attention to how molecular targets are arranged allows molecular- and interfacial-level recognitions to be combined.

We hope that this article provides a new perspective on biomaterial design. We wish to convince the reader that the binding character of a molecular or nanoscale adhesion element need not be the constraining factor in biomaterial performance. Attention to the arrangement and presentation of immobilized biomolecular fragments on surfaces whose other properties can be tuned comprises a means for the net surface interaction to outperform the individual surface elements. For instance, we prompt a reconsideration of the design rule that the optimal placement of receptors is on tethers that always place them forward of a support. Bringing molecular ligands the appropriate distance from the support will enable the discrimination of targets with different concentrations and arrangements of the molecular counterpart on their surfaces.

As a final point, we note that our original conception of multivalency followed from examples in biology. Although we have demonstrated this behavior with the simplest (electrostatic, rigid surfaces) example that we could devise, we believe that interfacial multivalency and threshold behavior are important for cells. In cells, the attractive and repulsive interactions differ in origin from the electrostatics showcased here. Also, the controlling factors for the contact area (at short times) are likely to include cell shape, modulus, roughness, and glycocalyx compressibility, allowing different cell types to be discriminated despite the presence of similar adhesion molecules. To best engineer this next level of sophistication into biomaterials, however, there is the need to better understand the energy landscapes of cell surfaces at length scales from 50 to 100 nm (the size of the contact zone). We need a quantitative understanding of the arrangement of attractive and repulsive functionalities in order to devise quantitative design targets for biomaterial design.

Acknowledgment. This work was made possible by support from NSF CBET-0428455 and the UMass MRSEC on Polymers: DMR-0213695. V.M.R. acknowledges support from NIH-GM-077173.

LA802554S